

# Al<sub>2</sub>O<sub>3</sub>-coated Fe<sub>3</sub>O<sub>4</sub>/graphene/TiO<sub>2</sub> hybrid nanocomposite mixture as anode material for lithium-ion batteries

K. Saravanakumar<sup>1,\*</sup>, J. Samson Isaac<sup>2</sup> and R. Rajesh<sup>3</sup>

<sup>1</sup>Department of Instrumentation and Control Engineering, Sri Krishna College of Technology, Coimbatore 641 042, India

<sup>2</sup>Department of Biomedical Engineering, Karunya Institute of Technology, Coimbatore 641 114, India

<sup>3</sup>Department of Engineering Design, Indian Institute of Technology Madras, Chennai 600 036, India

**Lithium-ion batteries are efficient energy storage devices in electric vehicles (EVs). Graphite is used in these batteries as an anode material because of its high stability and good conductivity. However, the need for stability, safety and reversibility is increasing rapidly in commercial EVs. In this study, a Fe<sub>3</sub>O<sub>4</sub>/TiO<sub>2</sub>/graphene hybrid nanocomposite coated with Al<sub>2</sub>O<sub>3</sub> has been developed using the microwave-assisted hydrothermal process with graphite as the anode material for lithium-ion batteries. This combination of nanomaterials increases the stability of the anode, electrical conductivity and electrochemical performance. The Fe<sub>3</sub>O<sub>4</sub>/graphene/TiO<sub>2</sub> nanocomposite results in a reversible capacity of 920 mAh g<sup>-1</sup> after analysing it in 160 cycles at a current density of 100 mAh g<sup>-1</sup>. The nanocomposite provides excellent long-term cycle stability of 650 mAh g<sup>-1</sup> after 160 cycles. This shows an ultrahigh rate capability of 475 mAh g<sup>-1</sup> at 150°C. The graphene and Fe<sub>3</sub>O<sub>4</sub>/graphene/TiO<sub>2</sub> hybrid nanocomposite mixture coated with Al<sub>2</sub>O<sub>3</sub> exhibits good nonlinear cumulative effects, stability, high reversibility, and increased ultrahigh rate capability.**

**Keywords:** Electric vehicles, graphite anode, hybrid nanocomposite, lithium-ion batteries, microwave-assisted hydrothermal process.

LITHIUM-ion batteries are the most preferred due to their long life, high stability, high rate capability and high energy density<sup>1-3</sup>. Graphite is widely used as a commercial anode material in all lithium-ion batteries due to its easy availability and low cost<sup>4,5</sup>. However, it is essential to find an alternative to meet the current demands of the automotive industry, which requires high energy capacity, safety and power density.

Fe<sub>3</sub>O<sub>4</sub> has an inverse spinel group structure and a high theoretical capacity of 924 mAh g<sup>-1</sup>, making it suitable as an anode material<sup>6</sup>. Fe<sub>3</sub>O<sub>4</sub> nanoparticles embedded in mesoporous carbon spheres display good cyclic stability at a current rate of 2000 mA g<sup>-1</sup> for 790 cycles, delivering a reversible capacity of 547.8 mAh g<sup>-1</sup> and a grape cluster-

like structured hybrid formed by Fe<sub>3</sub>O<sub>4</sub> nanoparticles. The carbon nanotubes have a reversible ability of 693 mAh g<sup>-1</sup> cycled at a current density of 300 mA g<sup>-1</sup> after 300 cycles.

Metal oxides cannot be used separately as an alternative for graphene because of their low rate capability and poor stability<sup>7</sup>. The performance of graphene can be improved by combining it with metal-oxide nanomaterials<sup>8</sup>. TiO<sub>2</sub> nanoparticles have good thermal and chemical properties<sup>9</sup>. Hence they are used in various research and industrial applications<sup>10</sup>. Al<sub>2</sub>O<sub>3</sub> nano-coating on the graphite anode material will act as a protective surface and provide proper safety against thermal runaways and ageing. It also prevents the risk of lithium metal deposition on the anode surface of aged lithium-ion batteries<sup>11</sup>.

Zhang *et al.*<sup>12</sup> developed an N-doped carbon nanotube/Fe<sub>3</sub>O<sub>4</sub> anode that produced excellent cycling stability with 87% capacity retention at 1 A g<sup>-1</sup> after 1000 cycles. Li *et al.*<sup>13</sup> developed a bio-inspired hierarchical nanofibrous Fe<sub>3</sub>O<sub>4</sub>/TiO<sub>2</sub>/carbon composite by applying a natural cellulose substance that showed very high electrochemical performances when used as an anode material for lithium-ion batteries.

In this study, we have developed a microwave-assisted hydrothermal method to make a Fe<sub>3</sub>O<sub>4</sub>/graphene/TiO<sub>2</sub> nanocomposite mixture coated with Al<sub>2</sub>O<sub>3</sub> (FGT-Al) for a lithium-ion battery. The graphene anode in the Fe<sub>3</sub>O<sub>4</sub>/TiO<sub>2</sub> mixture delivers excellent chemical and thermal performance. The FGT-Al anode has a reversible capacity of 7490 mAh g<sup>-1</sup> after 140 cycles, which is 92% of the first cycle capacity. Moreover, the material shows a relatively high discharge capacity of 656 mAh g<sup>-1</sup>. The nanocomposite exhibits cycle stability of 650 mAh g<sup>-1</sup> up to 140 cycles.

The significant contributions of this study are:

- The problem of poor cyclic stability in most anode materials is addressed here. Cycle tests up to 1400 cycles have been carried out and the obtained specific capacity was reported.
- Current density used 100 to 1600 mAh g<sup>-1</sup>, and specific capacity and improved reversibility are reported here.
- C values varied from 1 to 150, and the corresponding specific capacity was obtained to check the performance of the proposed anode material.

\*For correspondence. (e-mail: saravanakumar.k@skct.edu.in)

- Discharge and charge voltage profiles were acquired and the plateau was obtained to check the performance of the electrodes.

## Material synthesis and characterization

### Graphene synthesis

The synthesis of  $\text{Fe}_3\text{O}_4/\text{graphene}/\text{TiO}_2$  was carried out using the graphene synthesis method<sup>14</sup>. First, natural graphite flakes of specification 9% carbon,  $-100$  mesh ( $\geq 80\%$ ) were mixed with 50 ml of concentrated nitric acid at  $60^\circ\text{C}$  and 10 ml of hydrogen peroxide by magnetic stirring. This mixture was stirred and washed with deionized water to make it neutral.

The obtained graphite intercalation compounds were heated at  $150^\circ\text{C}$  for 24 h. The expanded graphite flakes were dispersed in 60 ml methanol solution. The obtained solution was transferred into a 100-ml Teflon-lined autoclave and the oven temperature was kept at  $200^\circ\text{C}$  for 20 h. Finally, the collected product was rewashed using deionized water and 10% HCL solution.

### Synthesis of $\text{Fe}_3\text{O}_4/\text{graphene}/\text{TiO}_2$

The synthesis of  $\text{Fe}_3\text{O}_4/\text{graphene}/\text{TiO}_2$  composites was done according to Lu *et al.*<sup>15</sup>. The prepared graphene (400 mg) and  $\text{FeCl}_3 \cdot 6\text{H}_2\text{O}$  (1200 mg) were dispersed into 60 ml of ethylene glycol solution with trisodium citrate (150 mg), sodium acetate (2000 mg) and polyethylene glycol Mn 20000 (1000 mg). The obtained mixture was transferred into a 100-ml Teflon-lined autoclave and the oven temperature was kept at  $200^\circ\text{C}$  for 20 h. Next, the  $\text{Fe}_3\text{O}_4/\text{graphene}/\text{TiO}_2$  mixture was synthesized.

The obtained  $\text{Fe}_3\text{O}_4/\text{graphene}$  composite was further treated by dispersing 0.5 g in 150 ml of absolute ethanol. The ethanol-dispersed composite was further mixed with 1.5 ml, 35% concentrated ammonia solution. An ultrasound-assisted synthesis process was used for this. The treated mixture was added to tetrabutyl titanate (TBOT, 1.5 ml) and the hydrolysis process was carried out for 36 h at  $60^\circ\text{C}$ .

The obtained mixture was washed thoroughly with deionized water and ethanol. Next, 40 ml of deionized water was added to  $\text{Fe}_3\text{O}_4/\text{graphene}/\text{TiO}_2$  composite and the product was transferred to an autoclave. Temperature maintained in the autoclave was about  $200^\circ\text{C}$  for 36 h. The product was cooled to  $25^\circ\text{C}$  and the nanocomposite mixture was washed and dried.

### Coating of $\text{Al}_2\text{O}_3$

The prepared composite acted as an anode for the Li-ion batteries. Friesen *et al.*<sup>16</sup> reported that the anode surface

could be coated with  $\text{Al}_2\text{O}_3$  nanoparticles directly by a wet coating process.

### Material characterization

The prepared anode material was tested using a field-emitted scanning electron microscope (Carl Zeiss Microscopy Ltd, UK and SIGMA, USA), and nanoscale analytics and elemental analysis were performed. Transmission electron microscopic (TEM) studies (JEOL JEM 2100 High-Resolution Transmission Electron Microscope) were performed and an energy dispersive X-ray spectrometer (EDX) with a  $0.28\text{sr}$  solid angle was used for highly sensitive analysis at nanometre resolution. Wide-angle X-ray diffraction (XRD) (Panalytical, The Netherlands and X'pert<sup>3</sup> Powder) was used for phase analysis and orientation of a single crystal or grain. Fourier transform infrared (FTIR) spectroscopy and Raman spectroscopy are interchangeable, but the latter is preferred in functional groups with weak dipole changes<sup>17</sup>.

In this study, we have used FTIR spectroscopy (System ReactIR 702L, TEMCT) to analyse the functional groups, which exhibited good dipole changes and a low degree of symmetry. X-ray photoelectron microscopy (XPS-PHI VersaProbe III Scanning XPS Microprobe, Physical Electronics, USA) was used for the complete electronic band structure characterization of the prepared nanocomposite anode.

## Results and discussion

The  $\text{Fe}_3\text{O}_4/\text{graphene}/\text{TiO}_2$  composite was synthesized using TBOT. TEM and scanning electron microscopic (SEM) analysis was performed on the obtained products.

From the TEM images, it can be observed that graphene and  $\text{TiO}_2$  are well synthesized with  $\text{Fe}_3\text{O}_4$  at nanoscale thickness. Figure 1 shows that  $\text{Fe}_3\text{O}_4$  and  $\text{TiO}_2$  nanoparticles are adequately fed on the surface of the graphene after

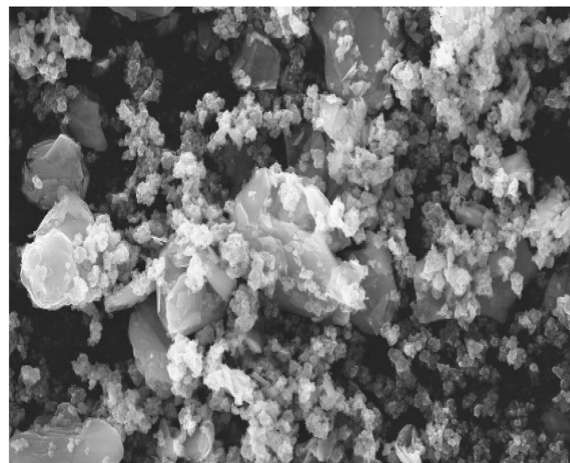


**Figure 1.** Scanning electron microscopic images of  $\text{Fe}_3\text{O}_4/\text{graphene}/\text{TiO}_2$ .

the hydrothermal process.  $\text{TiO}_2$  crystals are visible on the surface of the  $\text{Fe}_3\text{O}_4$ /graphene mixture.

EDX analysis was performed to determine the components and distribution in the  $\text{Al}_2\text{O}_3$ -coated  $\text{Fe}_3\text{O}_4$ /graphene/ $\text{TiO}_2$  composite. Figure 2 confirms that titanium dioxide, iron, aluminium, carbon and oxygen are present in the composite. The analysis indicates that Ti is distributed more than Fe, while the Fe distribution area is more than C and O. From the above observations, Ti and Al stay at the outer layer of the  $\text{Fe}_3\text{O}_4$  nanoparticles.  $\text{TiO}_2$  particles and aluminium coating are made on the  $\text{Fe}_3\text{O}_4$  and graphene particles. Table 1 shows the elemental analysis using EDX. The weight and atomic details of the elements present in the nanocomposite are provided in the table. The weight ratio of Ti, Al and Fe is 10 : 4.12 : 8.93.

Figure 3 shows the wide-angle XRD characterization of the prepared  $\text{Fe}_3\text{O}_4$ /graphene/ $\text{TiO}_2$  composite and  $\text{Al}_2\text{O}_3$ -coated  $\text{Fe}_3\text{O}_4$ /graphene/ $\text{TiO}_2$  composite. The  $\text{Al}_2\text{O}_3$ -coating is reflected in  $2\theta = 32, 40, 43, 62$  diffraction peaks. It is indexed at 220, 311, 400 and 440 reflections respectively. The Debye–Scherrer formula was used to estimate the nanocrystal size of the  $\text{Al}_2\text{O}_3$  nanoparticles as 40.25 nm.

Figure 4 shows the FTIR spectra of  $\text{Fe}_3\text{O}_4$ /graphene/ $\text{TiO}_2$  composite and  $\text{Al}_2\text{O}_3$ -coated  $\text{Fe}_3\text{O}_4$ /graphene/ $\text{TiO}_2$

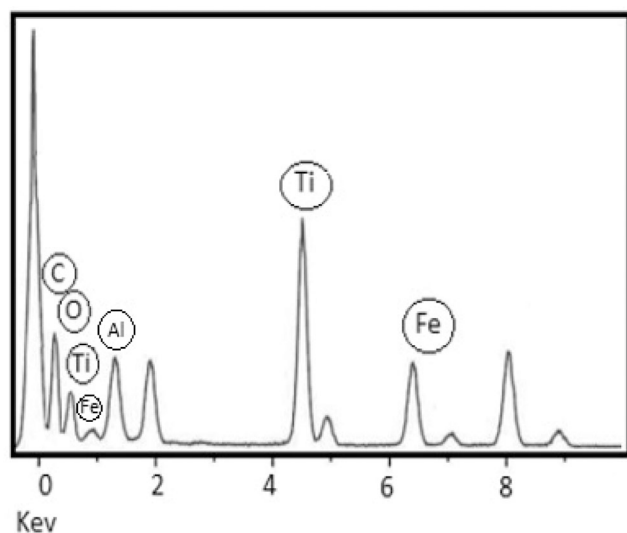


**Figure 2.** Energy dispersive X-ray spectroscopy analysis of  $\text{Al}_2\text{O}_3$ -coated  $\text{Fe}_3\text{O}_4$ /graphene/ $\text{TiO}_2$  composite.

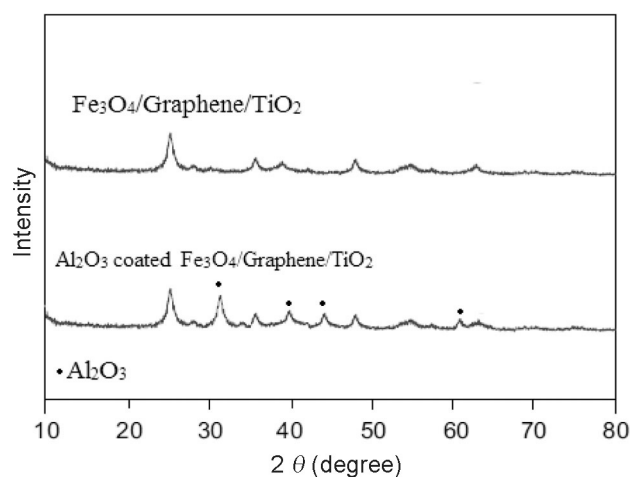
**Table 1.** EDX elemental analysis for weight and atomic percentage

Element	Weight (%)	Atomic percentage
O	25.1	35.2
C	21.6	25.6
Ti	15.64	10.5
Fe	6.84	6.25
Al	17.5	7.04
Cu	13.32	15.41

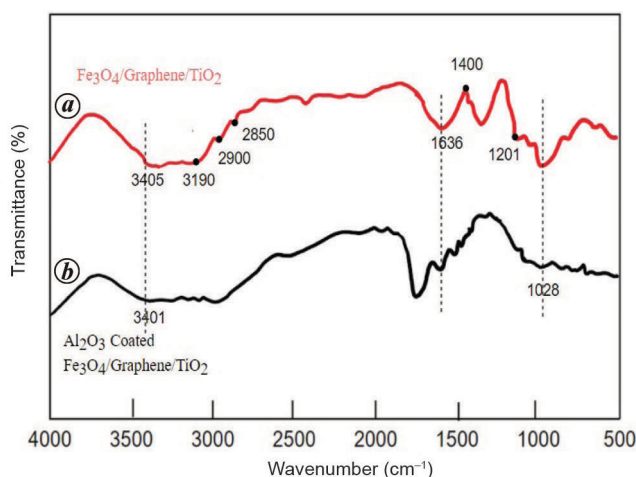
composite. The FTIR spectrum of  $\text{Al}_2\text{O}_3$ -coated  $\text{Fe}_3\text{O}_4$ /graphene/ $\text{TiO}_2$  differs from that of  $\text{Fe}_3\text{O}_4$ /graphene/ $\text{TiO}_2$  as recorded by the peaks at  $3400$  and  $1636\text{ cm}^{-1}$ . In Figure 4 *b*, the wavenumber obtained between  $3600$  and  $3100\text{ cm}^{-1}$  belongs to OH. The Al–O bonds are found at  $1100\text{ cm}^{-1}$  (ref. 18), Ti–O bonds at  $1650$  and  $600\text{ cm}^{-1}$  and Fe–O bonds at  $750\text{ cm}^{-1}$  (ref. 19).

Electronic band structure characterization was done using XPS spectra. Figure 5 *a* shows the complete XPS spectrum of the prepared nanocomposite. It contains O 1s, C 1s, Fe 2p<sub>1/2</sub>, Fe 2p<sub>3/2</sub>, Ti 2p and Al 2p. In Figure 5 *b*, the Ti 2p spectrum has been separately displayed.

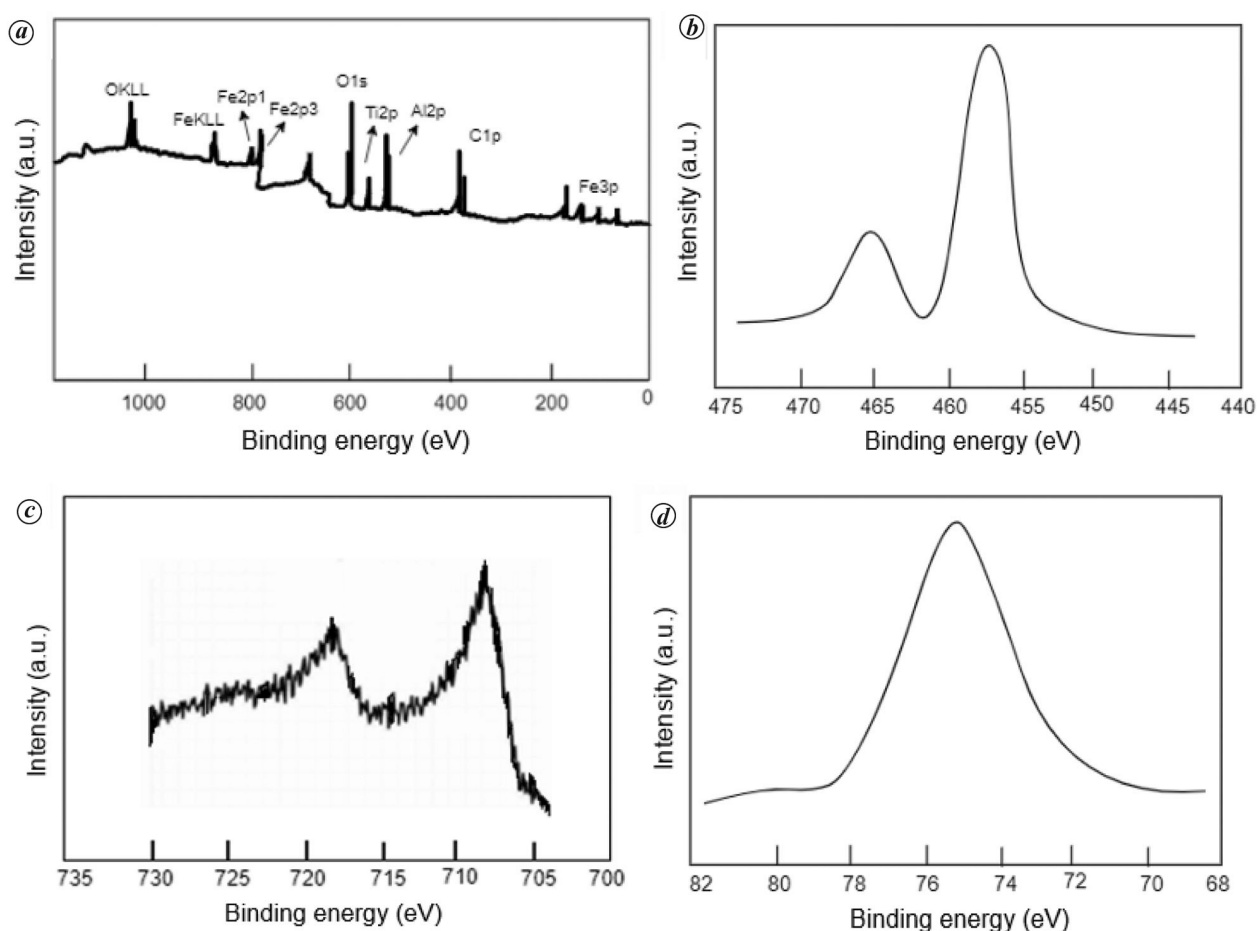
The binding energy increases due to the interaction between Ti and graphene<sup>20</sup>. Peaks obtained in Figure 5 *c* are located in the binding energy of  $710$  and  $725\text{ eV}$  approximately, to synthesize  $\text{Fe}_3\text{O}_4$  (ref. 21). In addition, Al 2p of the  $\text{Al}_2\text{O}_3$ -coated  $\text{Fe}_3\text{O}_4$ /graphene/ $\text{TiO}_2$  composite is taken at the binding energy of  $75\text{ eV}$  (ref. 22; Figure 5 *d*).



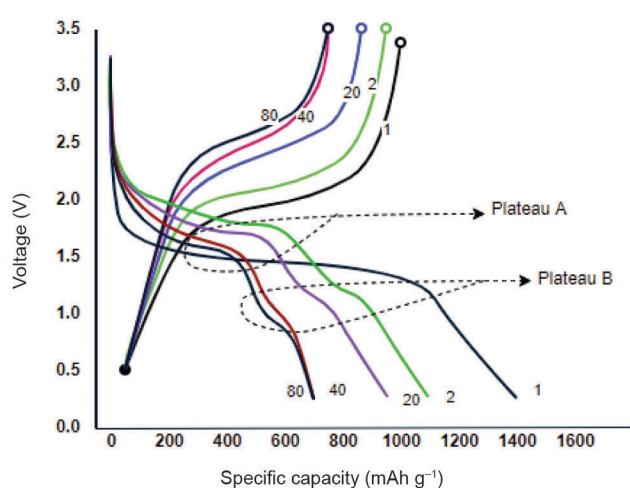
**Figure 3.** Wide-angle X-ray diffraction analysis of  $\text{Fe}_3\text{O}_4$ /graphene/ $\text{TiO}_2$  composite and  $\text{Al}_2\text{O}_3$ -coated  $\text{Fe}_3\text{O}_4$ /graphene/ $\text{TiO}_2$  composite.



**Figure 4.** *a*, Fourier transform infrared (FTIR) of  $\text{Fe}_3\text{O}_4$ /graphene/ $\text{TiO}_2$  composite. *b*,  $\text{Al}_2\text{O}_3$ -coated  $\text{Fe}_3\text{O}_4$ /graphene/ $\text{TiO}_2$  composite.



**Figure 5.** *a*, XPS survey spectrum of  $\text{Al}_2\text{O}_3$ -coated  $\text{Fe}_3\text{O}_4$ /graphene/ $\text{TiO}_2$  composite. *b*, Ti 2p. *c*, Fe 2p. *d*, Al 2p spectra.



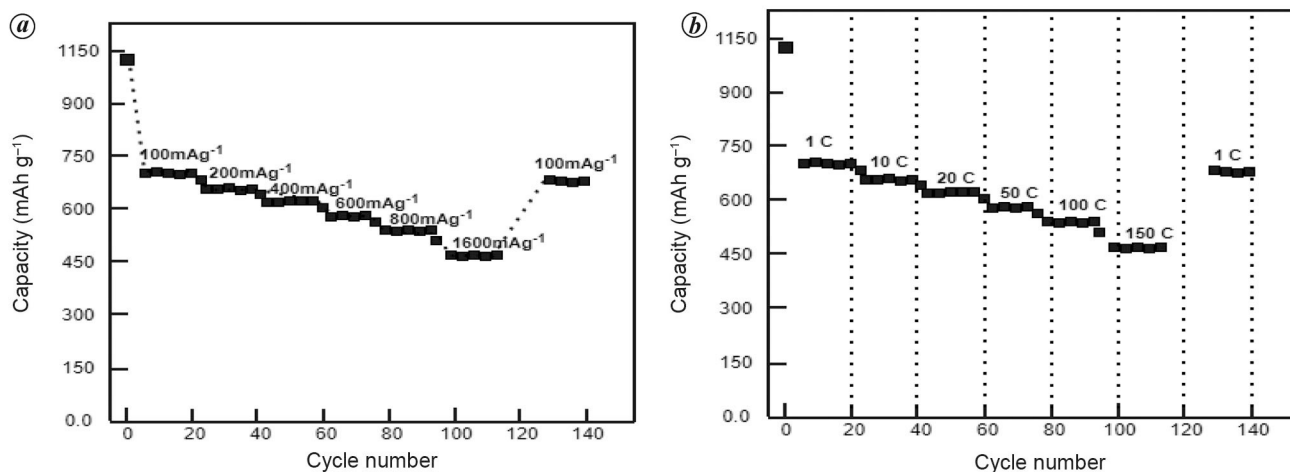
**Figure 6.** Discharge-charge voltage profiles of  $\text{Al}_2\text{O}_3$ -coated  $\text{Fe}_3\text{O}_4$ /graphene/ $\text{TiO}_2$  nanocomposite at different cycles.

Figure 6 shows the galvanostatic charge and discharge profile of  $\text{Al}_2\text{O}_3$ -coated  $\text{Fe}_3\text{O}_4$ /graphene/ $\text{TiO}_2$  composite electrode. Charge-discharge profiles were taken for 1st,

2nd, 20th, 40th and 80th cycles at a rate of  $160 \text{ mAh g}^{-1}$ . The first discharge shows the specific capacity of  $1400 \text{ mAh g}^{-1}$ . Tests carried out for the 2nd, 20th, 40th and 80th cycles gave a specific capacity of 1100, 950, 680 and  $675 \text{ mAh g}^{-1}$  respectively.

The charging-specific capacity of the  $\text{Al}_2\text{O}_3$ -coated  $\text{Fe}_3\text{O}_4$ /graphene/ $\text{TiO}_2$  composite was initially  $995 \text{ mAh g}^{-1}$ . In the second cycle, the specific capacity was reduced to  $935 \text{ mAh g}^{-1}$ . The 20th, 40th and 80th cycles displayed values of 800, 770 and  $675 \text{ mAh g}^{-1}$  respectively. Charge transfer resistance was reduced in the  $\text{Fe}_3\text{O}_4$ /graphene/ $\text{TiO}_2$  composite using  $\text{Al}_2\text{O}_3$  coating, which suppressed the growth of the solid electrolyte interphase<sup>23-25</sup>. The first set of the voltage plateau (plateau A) was observed at 1.5 V at initial discharge. The second discharge voltage plateau occurred at 1.8 V.

There was a slight increase in the voltage plateau for the second cycle compared to the first discharge cycle. At the 20th cycle, there was a further reduction in the voltage plateau at 1.7 V. At the 40th cycle, the voltage plateau occurred at 1.65 V. Finally, in the 80th cycle of discharge, the voltage plateau occurred at 1.6 V. The second voltage plateau (plateau B) occurred between 0.8 and 1.25 V.



**Figure 7.** *a*, Performance of the cell at different current densities. *b*, Rate capability of Al<sub>2</sub>O<sub>3</sub>-coated Fe<sub>3</sub>O<sub>4</sub>/graphene/TiO<sub>2</sub> from 1C to 150C.

The first charging curve showed a specific capacity of 1000, 950, 875, 750 and 650 mAh g<sup>-1</sup>, for the 2nd, 20th, 40th and 80th cycles respectively. The specific capacity of the battery decreased from the 1st cycle to the 80th cycle. At the 80th cycle, discharge specific capacity was 675 mAh g<sup>-1</sup> and charge capacity was 650 mAh g<sup>-1</sup>.

Figure 7 *a* shows the performance of the cell at different current densities. Initially, the specific capacity of the cell was 1100 mAh g<sup>-1</sup>. When the current density was 100 mA g<sup>-1</sup>, the cell exhibited a specific capacity of 685 mA g<sup>-1</sup>. The performance test was carried out for 200, 400, 600, 800 and 1600 mA g<sup>-1</sup>, and the cell had a specific capacity of 650, 625, 575, 525 and 475 mAh g<sup>-1</sup> respectively. When returning to the initial current density of 100 mA g<sup>-1</sup>, the cell had a specific capacity of 675 mAh g<sup>-1</sup>. At the beginning of the cycle test, at a current density of 100 mA g<sup>-1</sup>, the cell can have a specific capacity of 685 mAh g<sup>-1</sup>. When returning to the 140th cycle at various densities, it can have a specific capacity of 650 mAh g<sup>-1</sup>.

The Al<sub>2</sub>O<sub>3</sub>-coated Fe<sub>3</sub>O<sub>4</sub>/graphene/TiO<sub>2</sub> electrode had a reversible specific capacity of 525 mAh g<sup>-1</sup> at a nominal rate of 800 mA g<sup>-1</sup>. It had a capacity of 475 mAh g<sup>-1</sup> at a high rate of 1600 mA g<sup>-1</sup>. This shows the ability of the proposed anode to produce a very high specific capacity range at a high current density. When returning to the initial rate of 100 mA g<sup>-1</sup>, the Al<sub>2</sub>O<sub>3</sub>-coated Fe<sub>3</sub>O<sub>4</sub>/graphene/TiO<sub>2</sub> electrode reached a reversible specific capacity of 685 mAh g<sup>-1</sup>. It can be seen that the Al<sub>2</sub>O<sub>3</sub>-coated Fe<sub>3</sub>O<sub>4</sub>/graphene/TiO<sub>2</sub> electrode produces a competitive rate performance, excellent cycle stability and excellent reversibility.

Figure 7 *b* shows the rate capability, which is a critical parameter to determine the efficiency of the electrode. At a current rating of 1C, the average discharge capacity was 680 mAh g<sup>-1</sup>; at a current rating of 10C, the average discharge capacity was 650 mAh g<sup>-1</sup>, while at the current rat-

ings of 20C, 50C, 100C and 150C, the average discharge capacity was 625, 585, 550 and 475 mAh g<sup>-1</sup> respectively. Discharge capacity ranged from 685 to 675 mAh g<sup>-1</sup> at 1C, which is a good result compared to previous works mentioned in the literature. During the reversibility of current to 1C, the discharge capacity recovered to 675 mAh g<sup>-1</sup>. On average, the initial discharge capacity at 1C was 685 mAh g<sup>-1</sup>, and it could recover almost 98% during reversibility. Compared to previous works, Al<sub>2</sub>O<sub>3</sub>-coated Fe<sub>3</sub>O<sub>4</sub>/graphene/TiO<sub>2</sub> electrode exhibits a good reversible rate.

Figure 8 *a* shows the cyclic stability of the Al<sub>2</sub>O<sub>3</sub>-coated Fe<sub>3</sub>O<sub>4</sub>/graphene/TiO<sub>2</sub> nanoparticles. The graph clearly shows that after 110 cycles, the discharge capacity is 620 mAh g<sup>-1</sup>, which means the cyclic stability is very high compared to previous works. The Al<sub>2</sub>O<sub>3</sub>-coated Fe<sub>3</sub>O<sub>4</sub>/graphene/TiO<sub>2</sub> electrode exhibited a reversible capacity of 920 mAh g<sup>-1</sup> at a current density of 100 mAh g<sup>-1</sup> (Figure 8 *b*).

A performance analysis was carried out to confirm the quality of the prepared anode. Reversible capacity and cyclic stability of up to 160 cycles were checked. Current ratings up to 150°C were tested to estimate the rate capability of the anode. Cycle time was increased to more than 1400 to evaluate the stability of the anode for a longer cycle time. The prepared anode material gave much better results than similar nanoparticle compositions. Most of the nanoparticles provide good reversible capacity when a cycle is increased. However, they fail to withstand longer cycles.

To analyse the performance of the nanoparticles for a longer run, cyclic tests were carried out and results for reversible capacity were obtained. Figure 8 *c* shows that the Al<sub>2</sub>O<sub>3</sub>-coated Fe<sub>3</sub>O<sub>4</sub>/graphene/TiO<sub>2</sub> anode has a reversible capacity of 410 mAh g<sup>-1</sup> after 1400 cycles, showing excellent reversible ability and cyclic stability for a longer cycle rate.

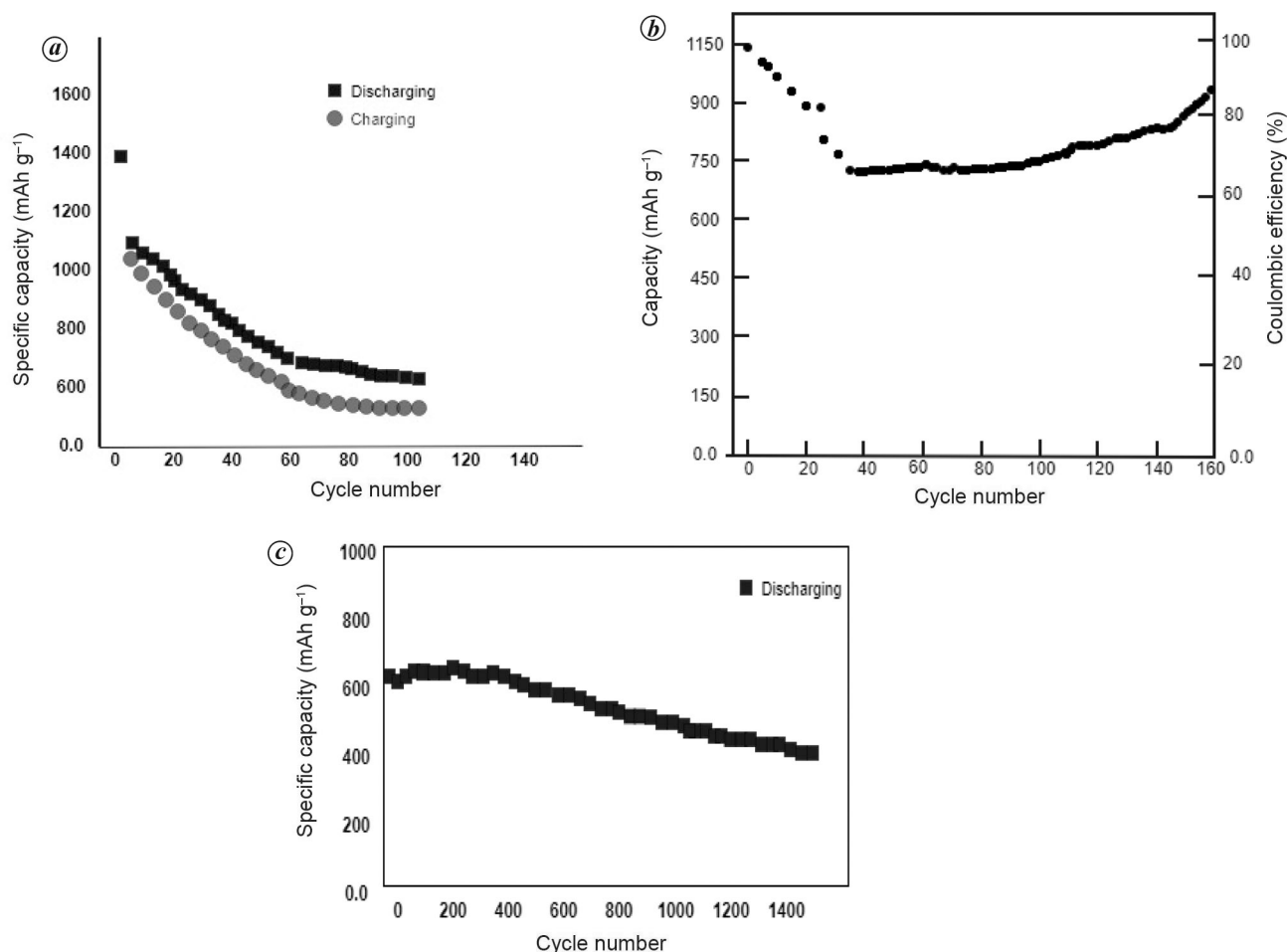


**Figure 8.** *a*, Cyclic stability of Al<sub>2</sub>O<sub>3</sub>-coated Fe<sub>3</sub>O<sub>4</sub>/graphene/TiO<sub>2</sub> nano-particles. *b*, Al<sub>2</sub>O<sub>3</sub>-coated Fe<sub>3</sub>O<sub>4</sub>/graphene/TiO<sub>2</sub> electrodes at current density of 100 mA h g<sup>-1</sup>. *c*, Cyclic stability of Al<sub>2</sub>O<sub>3</sub>-coated Fe<sub>3</sub>O<sub>4</sub>/graphene/TiO<sub>2</sub> nano-particles after 1400 cycles.

**Table 2.** Performance comparison between Al<sub>2</sub>O<sub>3</sub>-coated Fe<sub>3</sub>O<sub>4</sub>/graphene/TiO<sub>2</sub> anode (proposed work) and previous Fe<sub>3</sub>O<sub>4</sub>-based works

Anode materials	Cycle	Specific capacity (mAh g <sup>-1</sup> )	Current capacity (mAh g <sup>-1</sup> )
Fe <sub>3</sub> O <sub>4</sub> /graphene nanoparticles <sup>26</sup>	65	907	92.6
Hollow Fe <sub>3</sub> O <sub>4</sub> nanoparticles <sup>27</sup>	50	610	100
Carbon-confined Fe <sub>3</sub> O <sub>4</sub> nanoparticles	100	915	100
Proposed Al <sub>2</sub> O <sub>3</sub> -coated Fe <sub>3</sub> O <sub>4</sub> /graphene/TiO <sub>2</sub> nanoparticles	1000	350	1000
	160	920	100
	1400	410	1000

Specific capacity maintenance above 400 mA h g<sup>-1</sup> is a challenging task achieved in the proposed anode material. After 1400 cycles, the prepared anode material could still produce 410 mA h g<sup>-1</sup>, which is a good result compared to similar works. To confirm the performance of the prepared anode, the analysis report of the Al<sub>2</sub>O<sub>3</sub>-coated Fe<sub>3</sub>O<sub>4</sub>/graphene/TiO<sub>2</sub> electrode was compared with previous studies on Fe<sub>3</sub>O<sub>4</sub> nanoparticle-based anodes (Table 2). It is evident from Table 2 that the proposed anode exhibits a high performance rate and stability compared to previous works.

## Conclusion

The prepared Al<sub>2</sub>O<sub>3</sub>-coated Fe<sub>3</sub>O<sub>4</sub>/graphene/TiO<sub>2</sub> nano-composite was successfully tested as a lithium-ion battery anode. It showed good cycling stability and reversibility and Al<sub>2</sub>O<sub>3</sub> coating, which suppressed the growth of solid electrolyte interphase. Al<sub>2</sub>O<sub>3</sub>-coated Fe<sub>3</sub>O<sub>4</sub>/graphene/TiO<sub>2</sub> had a specific capacity of 920 mA h g<sup>-1</sup> after 160 cycles. The charging capacity of the cell also increased to 875 mA h g<sup>-1</sup> after 160 cycles. During performance analysis of the cell, it exhibited good stability and specific capacity

lies between 680 mAh g<sup>-1</sup> and 575 mAh g<sup>-1</sup> for current density variations between 100 mA g<sup>-1</sup> and 600 mA g<sup>-1</sup>. During the 140th cycle, the cell could still reverse a value of 650 mAh g<sup>-1</sup> at a current density of 100 mA g<sup>-1</sup>. Further improvement in the ratio of nanomaterials can help improve the performance of the lithium-ion battery anode.

- Zheng, M., Li, L., Gu, P., Lin, Z., Xue, H. and Pang, H., A glassy carbon electrode modified with ordered nanoporous Co<sub>3</sub>O<sub>4</sub> for non-enzymatic sensing of glucose. *Microchim. Acta*, 2017, **184**(3), 943–949.
- Wang, X., Wei, X. and Dai, H., Estimation of state of health of lithium-ion batteries based on charge transfer resistance considering different temperature and state of charge. *J. Energy Storage*, 2019, **21**, 618–631.
- Zhang, J. *et al.*, MOF-derived transition metal oxide encapsulated in carbon layer as stable lithium-ion battery anodes. *J. Alloys Compd.*, 2019, **797**, 83–91.
- Shen, L., Che, Q., Li, H. and Zhang, X., Mesoporous NiCo<sub>2</sub>O<sub>4</sub> nanowire arrays grown on carbon textiles as binder-free flexible electrodes for energy storage. *Adv. Funct. Mater.*, 2014, **24**(18), 2630–2637.
- Yuan, Y. F. *et al.*, NiCo<sub>2</sub>S<sub>4</sub> multi-shelled hollow polyhedrons as high-performance anode materials for lithium-ion batteries. *Electrochim. Acta*, 2019, **299**, 289–297.
- Han, J., Fu, Q., Xi, B., Ni, X., Yan, C., Feng, J. and Xiong, S., Loading Fe<sub>3</sub>O<sub>4</sub> nanoparticles on paper-derived carbon scaffold toward advanced lithium–sulfur batteries. *J. Energy Chem.*, 2021, **52**, 1–11.
- Ma, J. and Liu, C., Turning waste into treasure: reuse of contaminant-laden adsorbents (Cr(vi)-Fe<sub>3</sub>O<sub>4</sub>/C) as anodes with high potassium-storage capacity. *J. Colloid Interface Sci.*, 2021, **582**, 1107–1115.
- Shen, H., Xia, X., Yan, S., Jiao, X., Sun, D., Lei, W. and Hao, Q., SnO<sub>2</sub>/NiFe<sub>2</sub>O<sub>4</sub>/graphene nanocomposites as anode materials for lithium ion batteries. *J. Alloys Compd.*, 2021, **853**, 157017.
- Liu, Z. *et al.*, Sandwich shelled TiO<sub>2</sub>@Co<sub>3</sub>O<sub>4</sub>@Co<sub>3</sub>O<sub>4</sub>/C hollow spheres as anode materials for lithium ion batteries. *Chem. Commun.*, 2021, **57**(14), 1786–1789.
- Kumar, A., Hussain, I., Kumar, S. and Koo, B. H., Structural, optical properties and the origin of spin functionality in the Co modified TiO<sub>2</sub> nanoparticles. *Vacuum*, 2021, **183**, 109870.
- Friesen, A. *et al.*, Al<sub>2</sub>O<sub>3</sub> coating on anode surface in lithium ion batteries: impact on low temperature cycling and safety behavior. *J. Power Sources*, 2017, **363**, 70–77.
- Zhang, G., Li, X., Liu, H. and Wei, D., Engineering capacitive contribution in dual carbon-confined Fe<sub>3</sub>O<sub>4</sub> nanoparticle enabling superior Li<sup>+</sup> storage capability. *J. Mater. Sci.*, 2021, **56**(8), 5100–5112.
- Li, S., Wang, M., Luo, Y. and Huang, J., Bio-inspired hierarchical nanofibrous Fe<sub>3</sub>O<sub>4</sub>-TiO<sub>2</sub>-carbon composite as a high-performance anode material for lithium-ion batteries. *ACS Appl. Mater. Interfaces*, 2016, **8**(27), 17343–17351.
- Al-Hazmi, F. S., Al-Harbi, G. H., Beall, G. W., Al-Ghamdi, A. A., Obaid, A. Y. and Mahmoud, W. E., One pot synthesis of graphene-based on microwave assisted solvothermal technique. *Synth. Met.*, 2015, **200**, 54–57.
- Lu, J., Deng, C., Zhang, X. and Yang, P., Synthesis of Fe<sub>3</sub>O<sub>4</sub>/graphene/TiO<sub>2</sub> composites for the highly selective enrichment of phosphopeptides from biological samples. *ACS Appl. Mater. Interfaces*, 2013, **5**(15), 7330–7334.
- Friesen, A. *et al.*, Al<sub>2</sub>O<sub>3</sub> coating on anode surface in lithium-ion batteries: impact on low temperature cycling and safety behavior. *J. Power Sources*, 2017, **363**, 70–77.
- Jorio, A. and Saito, R., Raman spectroscopy for carbon nanotube applications. *J. Appl. Phys.*, 2021, **129**(2), 021102.
- González-Gómez, M. A. *et al.*, Development of superparamagnetic nanoparticles coated with polyacrylic acid and aluminum hydroxide as an efficient contrast agent for multimodal imaging. *Nanomaterials*, 2019, **9**(11), 1626.
- Nguyen, K. D. V. and Vo, K. D. N., Magnetite nanoparticles–TiO<sub>2</sub> nanoparticles–graphene oxide nanocomposite: synthesis, characterization and photocatalytic degradation for rhodamine-B dye. *AIMS Mater. Sci.*, 2020, **7**(3), 288–301.
- Wang, W., Xiao, K., Zhu, L., Yin, Y. and Wang, Z., Graphene oxide supported titanium dioxide and ferromagnetic oxide hybrid, a magnetically separable photocatalyst with enhanced photocatalytic activity for tetracycline hydrochloride degradation. *RSC Adv.*, 2017, **7**(34), 21287–21297.
- Tang, S. *et al.*, Fe<sub>3</sub>O<sub>4</sub> nanoparticles three-dimensional electro-peroxydisulfate for improving tetracycline degradation. *Chemosphere*, 2021, **268**, 129315.
- Cañón, J. and Teplyakov, A. V., XPS characterization of cobalt impregnated SiO<sub>2</sub> and  $\gamma$ -Al<sub>2</sub>O<sub>3</sub>. *Surf. Interface Anal.*, 2021, **53**(5), 475–481.
- Zhu, H., Shiraz, M. H. A., Liu, L., Hu, Y. and Liu, J., A facile and low-cost Al<sub>2</sub>O<sub>3</sub> coating as an artificial solid electrolyte interphase layer on graphite/silicon composites for lithium-ion batteries. *Nanotechnology*, 2021, **32**(14), 144001.
- Sumathi, S., Rajesh, R. and Subburaj, P., Investigation of dielectric strength of transformer oil based on hybrid TiO<sub>2</sub>/Al<sub>2</sub>O<sub>3</sub>/MoS<sub>2</sub> nanofluid using Taguchi and response surface methodology. *IETE J. Res.*, 2019, 1–9.
- Rajesh, R. and Sumathi, S., Certain performance investigation on hybrid TiO<sub>2</sub>/Al<sub>2</sub>O<sub>3</sub>/MoS<sub>2</sub> nanofiller coated 3 $\phi$  induction motor: a Taguchi and RSM based approach. *Energy Rep.*, 2020, **6**, 1638–1647.
- Jing, L., Fu, A., Li, H., Liu, J., Guo, P., Wang, Y. and Zhao, X. S., One-step solvothermal preparation of Fe<sub>3</sub>O<sub>4</sub>/graphene composites at elevated temperature and their application as anode materials for lithium-ion batteries. *RSC Adv.*, 2014, **4**(104), 59981–59989.
- Gao, G. *et al.*, PEG-200-assisted hydrothermal method for the controlled-synthesis of highly dispersed hollow Fe<sub>3</sub>O<sub>4</sub> nanoparticles. *J. Alloys Compd.*, 2013, **574**, 340–344.

Received 8 October 2021; revised accepted 12 May 2022

doi: 10.18520/cs/v123/i2/177-183